Supporting Information

Contrasting Arene, Alkene, Diene, and Formaldehyde Hydrogenation in H-ZSM-5, H-SSZ-13, and H-SAPO-34 Frameworks during MTO

Mykela DeLuca, Christina Janes, David Hibbitts*

Department of Chemical Engineering, University of Florida, Gainesville, FL 32611, USA

*Corresponding author: hibbitts@che.ufl.edu

Table of Contents

S1. Details of Framework Structures and Convergence Criteria

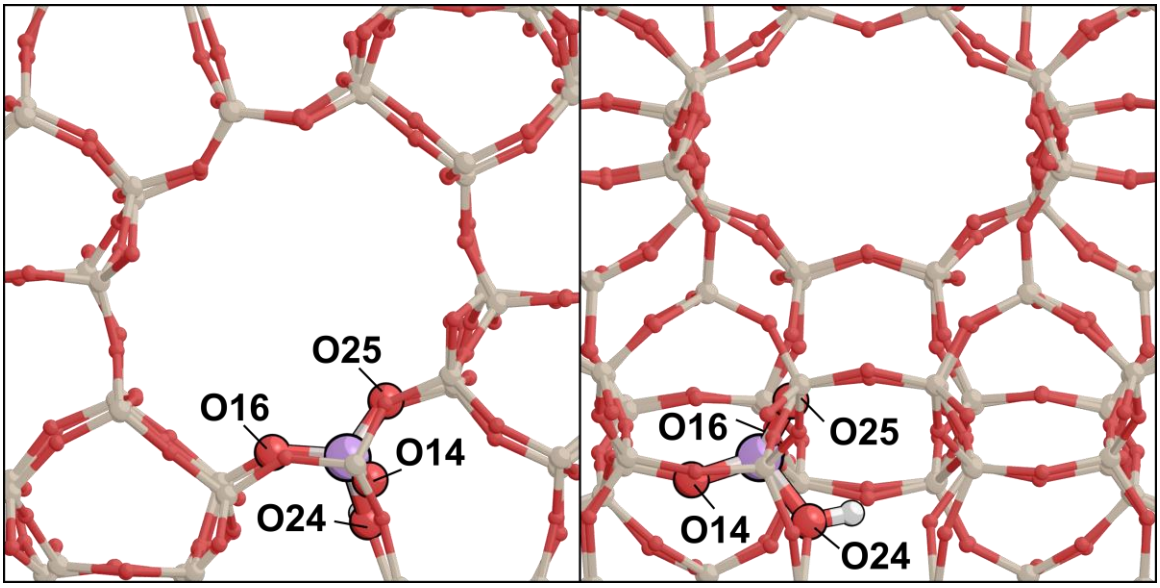

Figure S1. Straight (left) and sinusoidal (right) views of the H-ZSM-5 (MFI) structure.

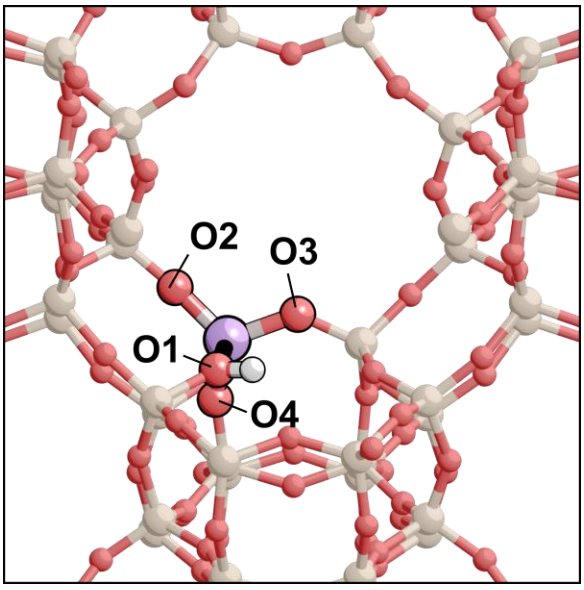

Figure S2. H-SSZ-13 (CHA) structure.

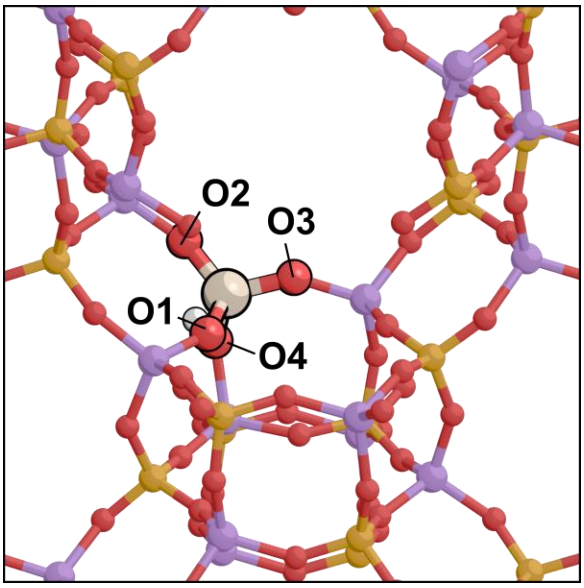

Figure S3. H-SAPO-34 (CHA) structure.

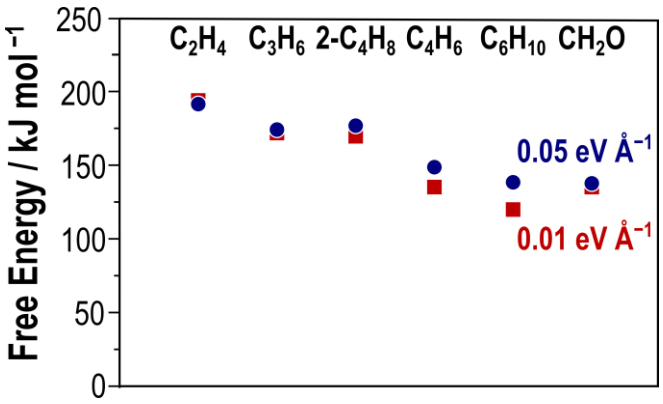

Figure S4. Free energies of hydrogenation transition states, relative to an empty zeolite, in H-SSZ-13 optimized to 0.05 eV $Å^{-1}$ (blue) and 0.01 eV $Å^{-1}$ (red).

S2. Additional information on hydrogenation rates and barriers

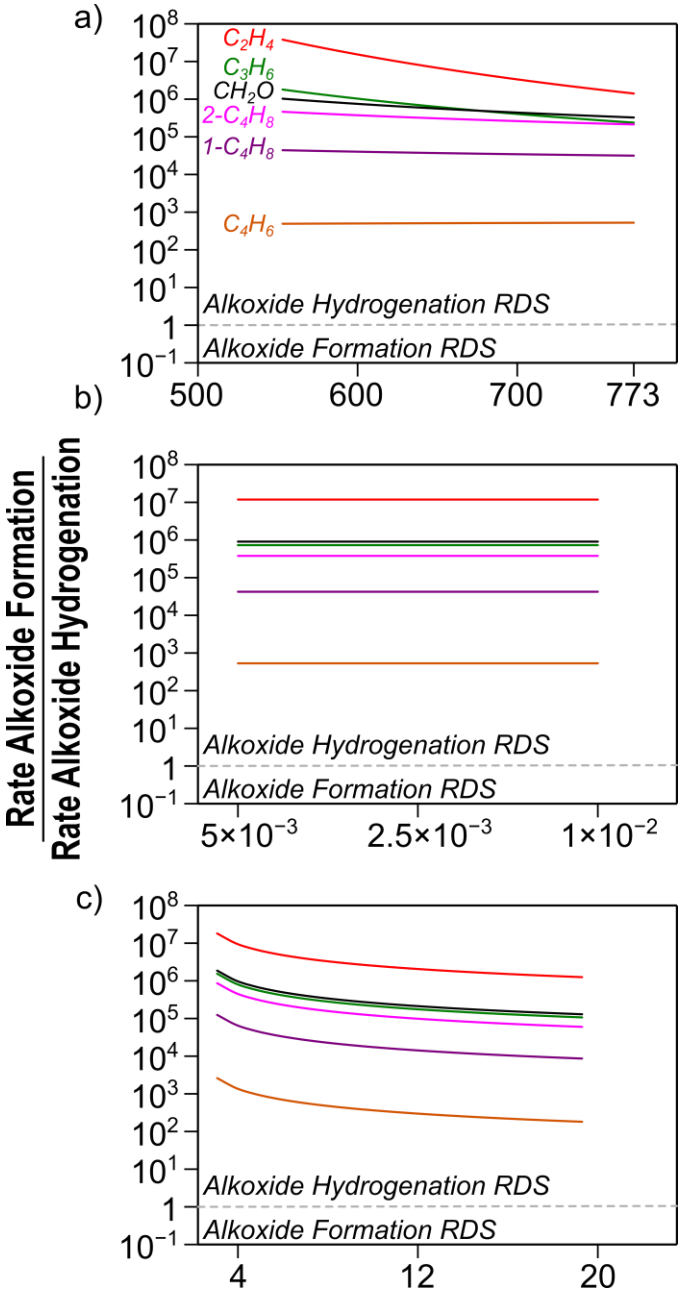

Figure S5. Ratio of alkoxide formation to alkoxide hydrogenation rates in H-ZSM-5 (MFI) reported from a) 553–773 K, b) 0.005–0.01 bar alkene, and c) 1–20 bar H_2. Rates are reported at 623 K, 16 bar H_2, and 0.001 bar alkene unless otherwise stated.

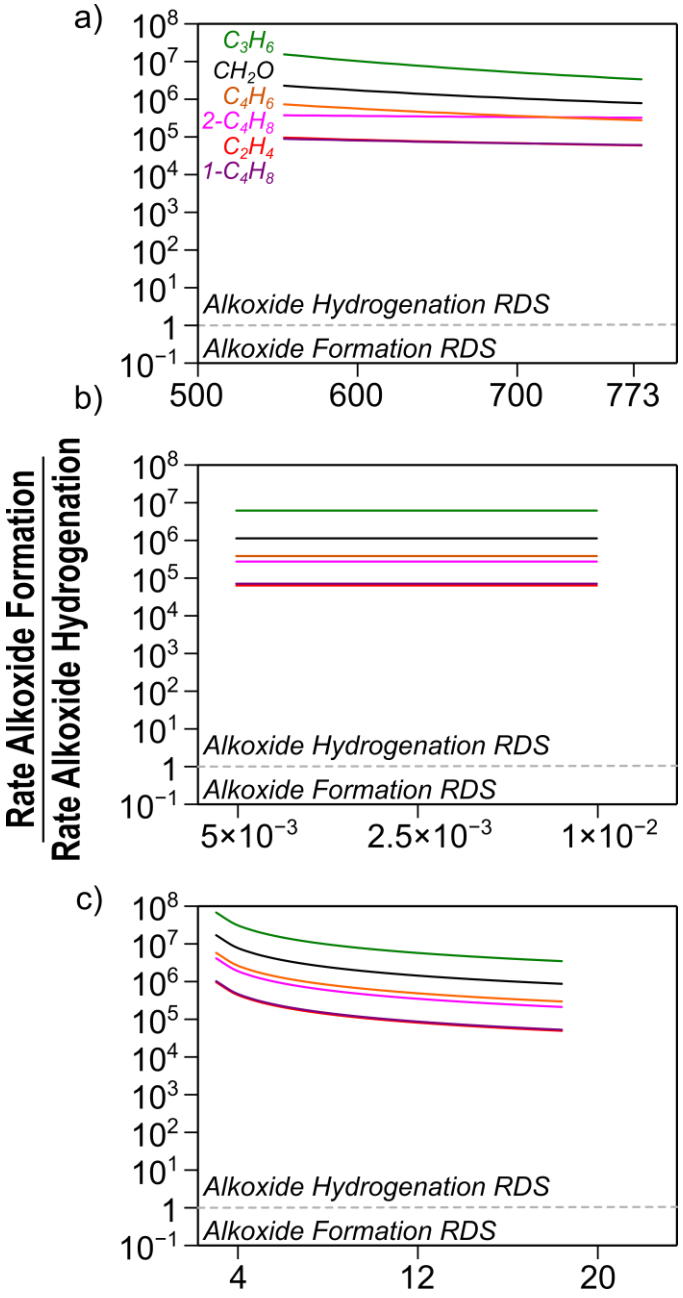

Figure S6. Ratio of alkoxide formation to alkoxide hydrogenation rates in H-SSZ-13 (CHA) reported from a) 553–773 K, b) 0.005–0.01 bar alkene, and c) 1–20 bar H_2. Rates are reported at 623 K, 16 bar H_2, and 0.001 bar alkene unless otherwise stated.

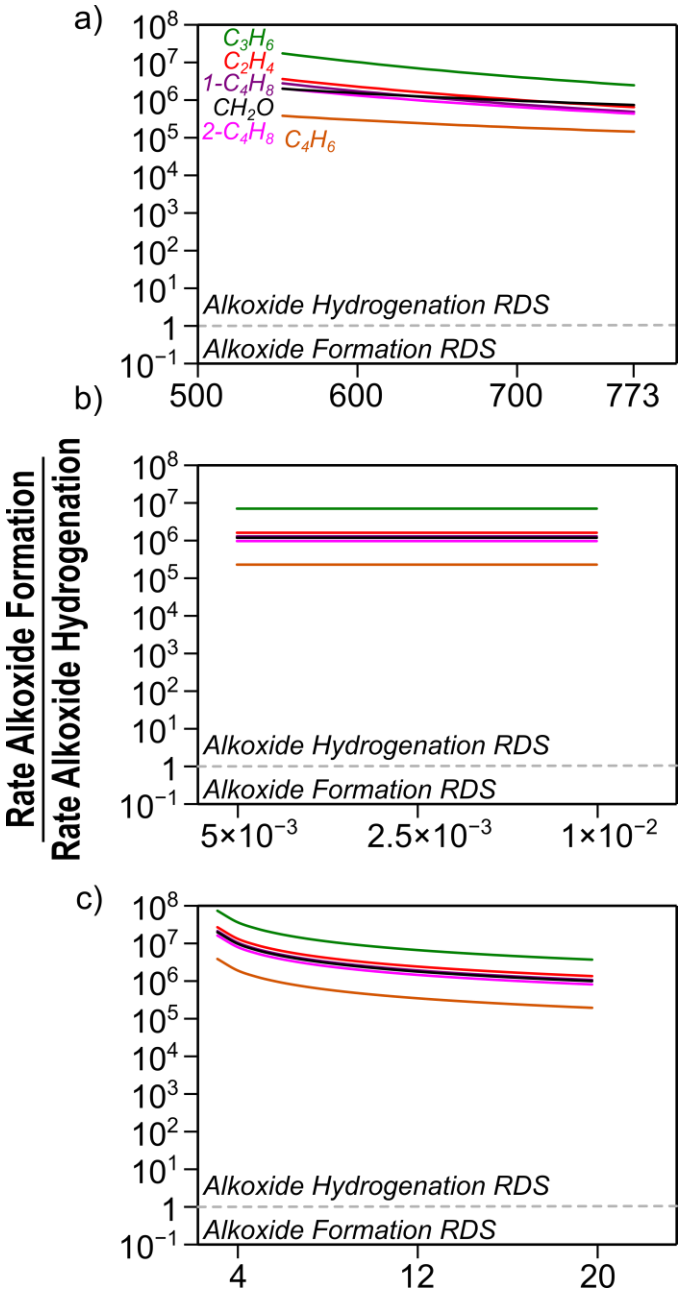

Figure S7. Ratio of alkoxide formation to alkoxide hydrogenation rates in H-SAPO-34 (CHA) reported from a) 553–773 K, b) 0.005–0.01 bar alkene, and c) 1–20 bar H_2. Rates are reported at 623 K, 16 bar H_2, and 0.001 bar alkene unless otherwise stated.

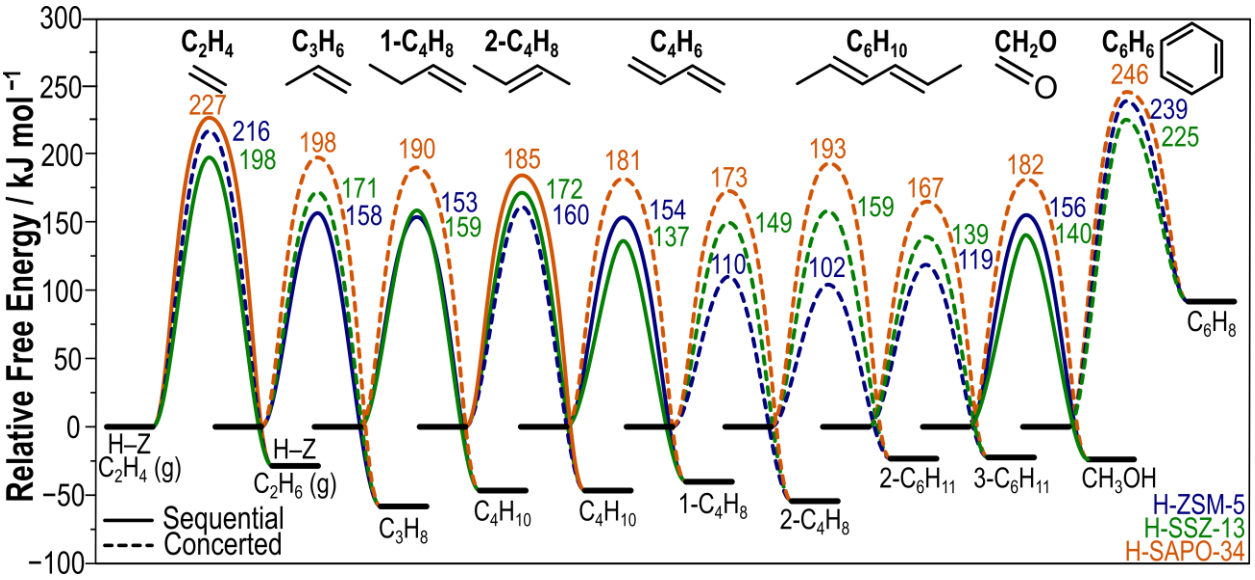

Figure S8. Reaction coordinate diagram of hydrogenation barriers in a) H-ZSM-5 (blue), b) H-SSZ-13 (green), and c) H-SAPO-34 using the BEEF-vdw functional.

S3. Temperature-corrected entropies and enthalpies

Frequency calculations were performed on all optimization and Dimer calculations. Frequency calculations are normal mode analyses and are used to determine zero-point vibrational energy (ZPVE), vibrational enthalpy (H_{vib}), and vibrational free energy (G_{vib}) for adsorbed species to calculate enthalpy (H):

$$H = E_0 + ZPVE + H_{vib} \quad \text{(S1)}$$

and free energies (G):

$$G = E_0 + ZPVE + G_{vib} \quad \text{(S2)}$$

Translational and rotational enthalpies and free energies are also calculated for gas phase species to determine gas phase enthalpy:

$$H = E_0 + ZPVE + H_{vib} + H_{rot} + H_{trans} \quad \text{(S3)}$$

and gas phase free energies:

$$G = E_0 + ZPVE + G_{vib} + G_{rot} + G_{trans} \quad \text{(S4)}$$

Low modes of frequency calculations, corresponding to frustrated rotates and translations within the zeolite pore, contribute significantly to entropy and enthalpy calculations (Eq. S32)—as such frequencies below 60 cm^{-1}, typically corresponding to frustrated rotation and translation, have been replaced with 60 cm^{-1} as discussed in the manuscript. Examination of the frequency calculations of the most favorable ethene (sequential), propene (concerted), 2-butene (sequential), butadiene (concerted), hexadiene (concerted), benzene (concerted), and formaldehyde (sequential) hydrogenation transition states in H-SSZ-13 demonstrate that, at most, 3 modes are replaced (Table S1, showing the 20 lowest modes of each transition state). Additionally, we have examined the free energies of the same transition states and varied the cutoff to only replace modes below 20

cm^{-1} with 20 cm^{-1}, modes below 100 cm^{-1} with 100 cm^{-1}, and no mode replacement. The free energy values vary slightly amongst the different cutoffs; however, the trends observed do not change with different cutoff values (Fig. S9).

Table S1. Twenty lowest frequencies of critical hydrogenation transition sates in H-SSZ-13

C_2H_4	C_3H_6	2-C_4H_8	C_4H_6	C_6H_{10}	C_6H_6	CH_2O
Seq.	*Conc.*	*Seq.*	*Conc.*	*Conc.*	*Conc.*	*Seq.*
562	422	412	494	365	531	826
531	409	409	406	325	481	740
503	387	381	385	315	474	652
410	367	366	366	271	434	580
379	328	331	324	260	396	547
365	295	274	297	252	360	498
332	271	271	272	221	323	450
316	267	257	260	214	299	370
297	241	225	247	206	276	350
268	231	215	222	198	261	286
260	211	209	217	181	219	271
225	206	201	203	165	215	265
223	201	157	193	130	205	231
207	189	133	161	86	131	227
170	107	105	101	72	109	197
159	88	89	65	61	73	169
129	59[a]	78	55[a]	50[a]	60	146
68	54[a]	48[a]	33[a]	47[a]	51[a]	72
60	-36[a]	36[a]	-17[a]	-33[a]	37[a]	55[a]
-396[b]	-231[b]	-243[b]	-293[b]	-420[b]	-320[b]	-597[b]

[a] Red values represent frequencies replaced with −60 cm^{-1}, [b] blue values represent the strongly negative mode of the transition state.

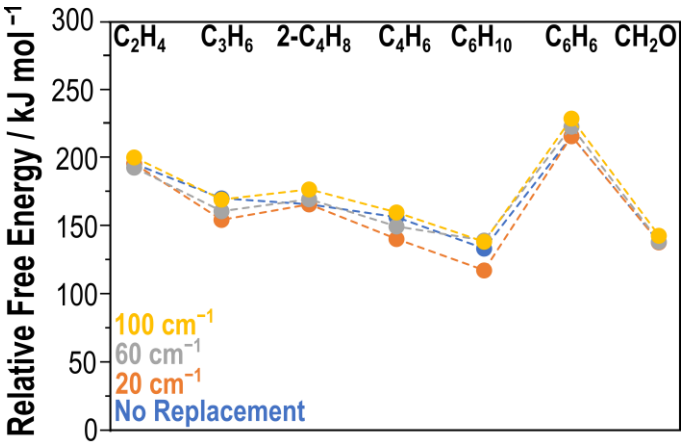

Figure S9. Free energy value (relative to an empty zeolite) of the sequential ethene, concerted propene, sequential 2-butene, concerted butadiene, concerted hexadiene, concerted benzene, and sequential formaldehyde hydrogenation transition states in H-SSZ-13 while varying the low-cut

off mode replacement to 100 cm^{-1} (yellow), 60 cm^{-1} (gray), 20 cm^{-1} (orange), and no mode replacement (blue). Free energy values (kJ mol^{-1}) are reported at 623 K.

S4. Details of Gas Phase Hydrogenation Thermodynamics

Table S2. Experimentally and theoretically obtained heats of hydrogenation.

	Temperature *K*	ΔH_{rxn} *Exp.*	ΔH_{rxn} *DFT*
$C_2H_4 + H_2 \rightarrow C_2H_6$	298	−136	−154
$C_3H_6 + H_2 \rightarrow C_3H_8$	298	−125	−139
$1\text{-}C_4H_8 + H_2 \rightarrow C_4H_{10}$	355	−126	−139
$2\text{-}C_4H_8 + H_2 \rightarrow C_4H_{10}$	355	−115	−123

S5. Maximum Rate Analysis of Hydrogenation Reactions

This analysis assumes that the potential most abundant surface intermediates (MASI) are empty sites (*), C_nH_{2n}*, and C_nH_{2n+1}–Z leading to a site balance of:

$$\frac{[*]}{[L]} = \left(1 + K_{C_nH_{2n}}(C_nH_{2n}) + K_{C_nH_{2n}}K_{S1}(C_nH_{2n})\right)^{-1} \quad \text{(S5)}$$

Where K_{S1} represents the quasi-equilibrated rate constant of alkoxide formation and species in parentheses indicate partial pressures.

There are three reaction steps associated with concerted hydrogenation and only one possible rate-determining step:

1. Alkene adsorption

$$C_nH_{2n}(g) + * \rightleftharpoons C_nH_{2n}^* \qquad K_{C_nH_{2n}} \quad \text{(S6)}$$

2. Hydrogen adsorption

$$C_nH_{2n}^* + H_2\,(g) \rightleftharpoons H_2 - C_nH_{2n}^* \qquad K_{H_2} \quad \text{(S7)}$$

3. Concerted reaction

$$H_2 - C_nH_{2n}^* \rightarrow C_nH_{2n+2} \qquad k_C \quad \text{(S8)}$$

Resulting in a product formation rate of

$$r = k_C[H_2 - C_nH_{2n}^*] \quad \text{(S9}$$

The rate described in equation S5 can be written in terms of partial pressures of each reactant by combining Eqs. S2, S3, and S5.

$$r = K_{C_nH_{2n}}K_{H_2}k_C(C_nH_{2n})(H_2)(*) \quad \text{(S10)}$$

Finally, Eq. S6 can be normalized by the number of sites derived in Eq. S1 to yield a general form of concerted hydrogenation.

$$\frac{r}{L} = K_{C_nH_{2n}}K_{H_2}k_C(C_nH_{2n})(H_2)\left(\frac{[*]}{[L]}\right) \quad \text{(S11)}$$

There are two possible rate-determining steps associated with the sequential mechanism: alkoxide formation or alkoxide hydrogenation. Both are considered in the following rate derivations. If alkoxide hydrogenation is considered to be the rate-determining step, the rate equation is dependent only on alkene adsorption:

$$C_nH_{2n}(g) + * \rightleftharpoons C_nH_{2n}^* \qquad K_{C_nH_{2n}} \tag{S12}$$

$$C_nH_{2n}^* \rightarrow C_nH_{2n} - Z \qquad k_{S1} \tag{S13}$$

$$C_nH_{2n} - Z + H_2(g) \rightarrow H_2 - C_nH_{2n} - Z \qquad kinetically\ irrelevant \tag{S14}$$

$$H_2 - C_nH_{2n} - Z \rightarrow C_nH_{2n+2} \qquad kinetically\ irrelevant \tag{S15}$$

where steps labeled kinetically irrelevant are not considered in the kinetic analysis as they occur after the rate-determining step resulting in the following rate equation:

$$r = k_{S1}[C_nH_{2n}^*] \tag{S16}$$

which can be written in terms of reactant pressures and normalized by the number of sites:

$$\frac{r}{L} = K_{C_nH_{2n}} k_{S1} (C_nH_{2n}) \left(\frac{[*]}{[L]}\right) \tag{S17}$$

Alternatively, alkoxide hydrogenation step can be rate-determining in the sequential mechanism via assumption of the following reaction system:

$$C_nH_{2n}(g) + * \rightleftharpoons C_nH_{2n}^* \qquad K_{C_nH_{2n}} \tag{S18}$$

$$C_nH_{2n}^* \rightarrow C_nH_{2n} - Z \qquad K_{S1} \tag{S19}$$

$$C_nH_{2n} - Z + H_2(g) \rightarrow H_2 - C_nH_{2n} - Z \qquad K'_{H_2} \tag{S20}$$

$$H_2 - C_nH_{2n} - Z \rightarrow C_nH_{2n+2} \qquad k_{S2} \tag{S21}$$

resulting in a rate equation dependent on both alkene and hydrogen pressure, similar to that of concerted (Eq. S7)

$$\frac{r}{L} = K_{C_nH_{2n}} K'_{H_2} k_{S2} (C_nH_{2n})(H_2) \left(\frac{[*]}{[L]}\right) \tag{S22}$$

Section S6. Kinetic Isotope Effects

Table S3. Kinetic Isotope Effect of concerted and sequential ethene and butadiene hydrogenation

Reaction	Zeolite	k_H/k_D	
		Seq.	Conc.
$1\text{-}C_4D_8 + D_2 + D\text{–}Z \rightarrow C_4D_{10} + D\text{–}Z$	CHA	3.28	2.66
	MFI	2.44	2.62
	SAPO	2.44	3.22
$1\text{-}C_4D_8 + H_2 + D\text{–}Z \rightarrow C_4HD_9 + H\text{–}Z$	CHA	2.32	2.43
	MFI	1.61	1.71
	SAPO	1.70	1.89
$C_4D_6 + D_2 + D\text{–}Z \rightarrow C_4D_8 + D\text{–}Z$	CHA	1.99	2.52
	MFI	2.19	2.12
	SAPO	2.91	2.21
$C_4D_6 + H_2 + D\text{–}Z \rightarrow C_4HD_7 + H\text{–}Z$	CHA	1.17	1.38
	MFI	1.26	0.87
	SAPO	1.64	1.16

Rate constants of deuterated compounds were obtained by replacing the reduced mass in the statistical mechanics equations for ZPVE, H_{vib}, and G_{vib}

$$ZPVE = \sum_i \left(\frac{1}{2} \nu_i h\right) \tag{S23}$$

$$H_{vib} = \sum_i \frac{\left(\nu_i h e^{-\frac{\nu_i h}{kT}}\right)}{1-e^{-\frac{\nu_i h}{kT}}} \tag{S24}$$

$$G_{vib} = \sum_i -kTln\left(\frac{1}{1-e^{-\frac{\nu_i h}{kT}}}\right) \tag{S25}$$

where the vibrational frequency is calculated as

$$\nu_i = \frac{1}{2\pi}\sqrt{\frac{k}{\mu}} \tag{S26}$$

and μ represents the reduced mass. Differences in the vibrational frequencies and calculated ZPVE, H_{vib} and G_{vib} values between H and D compounds are shown in Table S4 for H_2 (g).

Table S4. Differences in frequency, enthalpy, and free energy values between H_2 and D_2

	Frequency *cm^{-1}*	ZPVE *eV*	H_{vib} *eV*	G_{vib} *eV*	H *eV*	G *eV*
H_2	4298	2.7×10^{-1}	2.6×10^{-5}	-2.6×10^{-6}	−6.31	−7.33
D_2	3039	1.9×10^{-1}	3.4×10^{-4}	-4.8×10^{-5}	−6.38	−7.50

Section S7. Energies of Reactant, Product, and Transition State Structures

Table S5. Energies of States in H-ZSM-5 (MFI), H-SSZ-13 (CHA), and H-SAPO-34 (CHA).

	H-ZSM-5				H-SSZ-13				H-SAPO-34			
State	ΔH^a	ΔG^b	ΔS^c	Num.	ΔH^a	ΔG^b	ΔS^c	Num.	ΔH^a	ΔG^b	ΔS^c	Num.
Z–H + H_2 (g) + C_xH_y (g)	0	0	0		0	0	0		0	0	0	
C_xH_y Energies												
C_2H_4* + H_2 (g)	−46	26	−116		−61	24	−136	212294	−48	31	−127	
C_3H_6* + H_2 (g)	−65	14	−128		−77	4	−130	220636	−68	16	−134	
1-C_4H_8* + H_2 (g)	−87	7	−151	215038	−88	19	−173	199020	−79	24	−166	
2-C_4H_8* + H_2 (g)	−84	4	−142		−82	13	−152	198825	−74	23	−155	
C_4H_6* + H_2 (g)	−75	9	−136	220263	−84	10	−152	212450	−71	26	−156	
C_6H_{10}* + H_2 (g)	−126	−13	−221	220385	−107	12	−191	212499	−100	19	−191	
C_6H_6* + H_2 (g)	−138	82	−353	220478	−87	−2	−137	214074	−81	8	−142	
CH_2O* + H_2 (g)	−70	11	−129	220423	−77	7	−134	214067	−63	22	−136	
Z–C_xH_y Energies												
Z–C_2H_5* + H_2 (g)	−79	17	−153	211801	−89	16	−168	214291	−82	23	−168	
Z–1-C_3H_7* + H_2 (g)	−76	22	−166	215052	−83	29	−179	223942	−74	38	−180	
Z–2-C_3H_7* + H_2 (g)	−80	22	−163	211831	−93	15	−173	212084	−78	34	−179	
Z–1-C_4H_9* + H_2 (g)	−83	36	−192	220192	−97	30	−204	214503	−78	43	−195	
Z–2-C_4H_9* + H_2 (g)	−64	47	−177		−87	32	−190	214540	−91	39	−188	
Z–1p-C_4H_7* + H_2 (g)	−79	25	−167		−92	18	−177	214471	−69	42	−179	
Z–1s-C_4H_7* + H_2 (g)	−66	38	−167		−67	43	−177	220773	−59	52	−179	
Z–2p-C_4H_7* + H_2 (g)	−44	30	−119	225840	−92	19	−178	225864	−84	27	−179	
Z–CH_2OH* + H_2 (g)	−64	36	−161	214777	−77	31	−172	214607	−65	39	−167	
Z–C_6H_{11}* + H_2 (g)	−84	45	−207	214747	–	–	–	–	–	–	–	
Z–C_6H_7* + H_2 (g)	252	341	−141		–	–	–	–	–	–	–	
Protonated States												
C_4H_7*+H_2 (g)	−30	78	−174	211893	–	–	–	–	–	–	–	
C_6H_{11}*+H_2 (g)	−98	8	−171	211885	–	–	–	–	–	–	–	
C_6H_7*+H_2 (g)	13	96	−33	211783	–	–	–	–	–	–	–	

Table S6. Energies of Transition States at 623K in H-ZSM-5 (MFI)

State	$\Delta H^{\ddagger}$[a]	$\Delta G^{\ddagger}$[b]	$\Delta S^{\ddagger}$[c]	ΔH_{rxn}[a]	ΔG_{rxn}[b]	ΔS_{rxn}[c]	Img.	Num.[d]
Z–H + H_2 (g) + C_xH_y (g)	0	0	0	0	0	0		201071
Concerted								
$C_2H_4 \rightarrow C_2H_6$	56	220	−264	100	141	−65	S10a	200020
$C_3H_6 \rightarrow C_3H_8$	17	174	−251	39	50	−17	S11a	200489
1-$C_4H_8 \rightarrow C_4H_{10}$	−1	174	−281	68	96	−45	S12a	215847
2-$C_4H_8 \rightarrow C_4H_{10}$	−1	161	−260	77	108	−50	S13a	200847
$C_4H_6 \rightarrow$ 1-C_4H_8	−12	162	−280	66	113	−75	S14a	239113
$C_4H_6 \rightarrow$ 2-C_4H_8	−26	135	−258	52	85	−53	S15a	240812
$C_6H_{10} \rightarrow$ 2-C_6H_{12}	−75	122	−317	40	100	−95	S16a	232580
$C_6H_{10} \rightarrow$ 3-C_6H_{12}	−74	126	−320	42	104	−99	S17a	239145
$C_6H_6 \rightarrow C_6H_8$	66	243	−284	141	184	−69	S18a	200669
$CH_2O \rightarrow CH_3OH$	−27	151	−285	33	89	−91	S19a	200881
Alkoxide Formation								
$C_2H_4 \rightarrow$Z–C_2H_5	20	118	−159	78	65	−43	–	214933
$C_3H_6 \rightarrow$ Z–1-C_3H_7	20	120	−161	96	85	−33	–	215056
$C_3H_6 \rightarrow$ Z–2-C_3H_7	−21	81	−163	56	45	−35	–	215140
1-$C_4H_8 \rightarrow$ Z–1-C_4H_9	8	116	−174	110	95	−24	–	215035
1-$C_4H_8 \rightarrow$ Z–2-C_4H_9	−18	93	−179	86	69	−29	–	215149
2-$C_4H_8 \rightarrow$ Z–2-C_4H_9	−9	92	−163	89	75	−21	–	215042
$C_4H_6 \rightarrow$ Z–1p-C_4H_7	38	144	−170	114	135	−34	–	215021
$C_4H_6 \rightarrow$ Z–1s-C_4H_7	−21	78	−158	69	55	−22	–	215027
$C_4H_6 \rightarrow$Z–2p-C_4H_7	−13	89	−164	65	98	−54	–	227882
$CH_2O \rightarrow$ Z–CH_2OH	−58	49	−172	19	12	−43	–	220866
Alkoxide Hydrogenation								
Z–$C_2H_5 \rightarrow C_2H_6$	−39	137	−283	19	74	−89	S20a	221465
Z–1-$C_3H_7 \rightarrow C_3H_8$	49	200	−241	124	109	−19	–	221444
Z–2-$C_3H_7 \rightarrow C_3H_8$	12	170	−253	104	92	−28	S21a	221450
Z–2-$C_4H_9 \rightarrow C_4H_{10}$	3	176	−277	68	80	−19	S22a	221093
Z–1p-$C_4H_7 \rightarrow$ 1-C_4H_8	76	237	−258	156	168	−19	S23a	221099
Z–1s-$C_4H_7 \rightarrow$ 1-C_4H_8	−12	154	−267	75	93	−29	S24a	229159
Z–1s-$C_4H_7 \rightarrow$ 2-C_4H_8	−21	144	−266	65	83	−28	S25a	231576
Z–2p-$C_4H_7 \rightarrow$ 2-C_4H_8	−22	151	−276	65	98	−54	S26a	229129
Z–$CH_2OH \rightarrow CH_3OH$	−39	137	−283	19	74	−89	S27a	229187

[a]Enthalpy and [b]free energies are reported in kJ mol^{-1}, [c]entropy is reported in J K^{-1} mol^{-1}, [d]references the proivded POSCAR/MODECAR files

Table S7. Energies of Transition States at 623 K in H-SSZ-13 (CHA)

State	$\Delta H^{\neq}$[a]	$\Delta G^{\neq}$[b]	$\Delta S^{\neq}$[c]	ΔH_{rxn}[a]	ΔG_{rxn}[b]	ΔS_{rxn}[c]	Img.	Num.[d]
Z–H + H_2 (g) + C_xH_y (g)	0	0	0	0	0	0		223949
Concerted								
$C_2H_4 \rightarrow C_2H_6$	31	208	−284	88	139	−82	S10b	220815
$C_3H_6 \rightarrow C_3H_8$	3	161	−254	84	112	−46	S11b	200895
1-$C_4H_8 \rightarrow C_4H_{10}$	−16	168	−294	73	120	−75	S12b	220840
2-$C_4H_8 \rightarrow C_4H_{10}$	4	178	−280	97	128	−50	S13b	220690
$C_4H_6 \rightarrow$ 1-C_4H_8	−11	164	−281	79	120	−65	S14b	221630
$C_4H_6 \rightarrow$ 2-C_4H_8	−21	150	−274	69	105	−58	S15b	211358
$C_6H_{10} \rightarrow$ 2-C_6H_{12}	−46	158	−328	64	106	−68	S16b	211364
$C_6H_{10} \rightarrow$ 3-C_6H_{12}	−72	139	−339	38	87	−79	S17b	229740
$C_6H_6 \rightarrow C_6H_8$	39	223	−294	130	186	−90	S18b	221631
$CH_2O \rightarrow CH_3OH$	−41	146	−300	41	99	−92	S19b	201013
Alkoxide Formation								
$C_2H_4 \rightarrow$Z–C_2H_5	10	117	−172	84	70	−36	–	214294
$C_3H_6 \rightarrow$ Z–1-C_3H_7	11	119	−173	98	88	−43	–	220638
$C_3H_6 \rightarrow$ Z–2-C_3H_7	−23	76	−158	69	54	−28	–	220662
1-$C_4H_8 \rightarrow$ Z–1-C_4H_9	−2	124	−201	97	86	−29	–	220680
1-$C_4H_8 \rightarrow$ Z–2-C_4H_9	−27	87	−183	75	61	−10	–	220704
2-$C_4H_8 \rightarrow$ Z–2-C_4H_9	−7	89	−155	86	74	−3	–	220739
$C_4H_6 \rightarrow$ Z–1p-C_4H_7	15	128	−182	110	99	−30	–	220742
$C_4H_6 \rightarrow$ Z–1s-C_4H_7	−39	69	−174	60	45	−22	–	220774
$C_4H_6 \rightarrow$Z–2p-C_4H_7	−43	65	−174	54	41	−22	–	227876
$CH_2O \rightarrow$ Z–CH_2OH	−63	48	−178	22	13	−44	–	221119
Alkoxide Hydrogenation								
Z–$C_2H_5 \rightarrow C_2H_6$	18	193	−281	127	106	−57	S20b	229190
Z–1-$C_3H_7 \rightarrow C_3H_8$	39	205	−265	140	125	−33	S21b	229193
Z–2-$C_3H_7 \rightarrow C_3H_8$	2	175	−278	96	129	−53	S22b	231485
Z–1-$C_4H_9 \rightarrow C_4H_{10}$	–	–	–	–	–	–	–	–
Z–2-$C_4H_9 \rightarrow C_4H_{10}$	−5	173	−285	75	61	−10	S23b	228906
Z–1p-$C_4H_7 \rightarrow$ 1-C_4H_8	62	241	−287	145	135	−39	S24b	228908
Z–1s-$C_4H_7 \rightarrow$ 1-C_4H_8	−24	152	−282	64	51	−33	S25b	228985
Z–1s-$C_4H_7 \rightarrow$ 2-C_4H_8	−23	155	−285	64	52	−37	S26b	230331
Z–2p-$C_4H_7 \rightarrow$ 2-C_4H_8	−15	159	−280	79	66	−47	S27b	229257
Z–$CH_2OH \rightarrow CH_3OH$	−46	138	−296	29	45	−75	S28b	230364

[a]Enthalpy and [b]free energies are reported in kJ mol^{-1}, [c]entropy is reported in J K^{-1} mol^{-1}, [d]references the proivded POSCAR/MODECAR files

Table S8. Energies of Transition States at 623 K in H-SAPO-34 (CHA)

State	$\Delta H^{\neq a}$	$\Delta G^{\neq b}$	$\Delta S^{\neq c}$	$\Delta H_{rxn}{}^{a}$	$\Delta G_{rxn}{}^{b}$	$\Delta S_{rxn}{}^{c}$	Img.	Num.[d]
Z–H + H_2 (g) + C_xH_y (g)	0	0	0	0	0	0		1195
Concerted								
$C_2H_4 \rightarrow C_2H_6$	50	230	−288	100	151	−81	S10c	1693
$C_3H_6 \rightarrow C_3H_8$	22	189	−268	96	126	−47	S11c	1877
1-$C_4H_8 \rightarrow C_4H_{10}$	−2	188	−304	83	124	−65	S12c	2254
2-$C_4H_8 \rightarrow C_4H_{10}$	34	212	−285	112	162	−80	S13c	2334
$C_4H_6 \rightarrow$ 1-C_4H_8	1	182	−290	72	113	−66	S14c	1944
$C_4H_6 \rightarrow$ 2-C_4H_8	−10	173	−294	60	104	−71	S15c	2252
$C_6H_{10} \rightarrow$ 2-C_6H_{12}	−34	171	−329	64	105	−67	S16c	2556
$C_6H_{10} \rightarrow$ 3-C_6H_{12}	−37	168	−326	60	102	−67	S17c	2314
$C_6H_6 \rightarrow C_6H_8$	65	245	−290	148	201	−84	S18c	1498
$CH_2O \rightarrow CH_3OH$	−32	152	−296	40	94	−88	S19c	2150
Alkoxide Formation								
$C_2H_4 \rightarrow$Z–C_2H_5	24	130	−170	72	99	−43	–	2049
$C_3H_6 \rightarrow$ Z–1-C_3H_7	26	135	−175	93	119	−41	–	1384
$C_3H_6 \rightarrow$ Z–2-C_3H_7	26	105	−175	64	89	−40	–	1399
1-$C_4H_8 \rightarrow$ Z–1-C_4H_9	14	138	−199	94	114	−33	–	1407
1-$C_4H_8 \rightarrow$ Z–2-C_4H_9	−8	110	−188	72	86	−23	–	1422
2-$C_4H_8 \rightarrow$ Z–2-C_4H_9	12	121	−175	85	98	−20	–	1439
$C_4H_6 \rightarrow$ Z–1p-C_4H_7	32	146	−184	103	120	−28	–	1442
$C_4H_6 \rightarrow$ Z–1s-C_4H_7	−16	94	−177	55	68	−21	–	1463
$C_4H_6 \rightarrow$Z–2p-C_4H_7	−16	95	−177	56	69	−21	–	2034
$CH_2O \rightarrow$ Z–CH_2OH	−45	67	−179	18	45	−43	–	1346
Alkoxide Hydrogenation								
Z–$C_2H_5 \rightarrow C_2H_6$	52	223	−274	132	168	−58	S20c	1761
Z–1-$C_3H_7 \rightarrow C_3H_8$	69	231	−260	235	235	1	S21c	1764
Z–2-$C_3H_7 \rightarrow C_3H_8$	28	205	−284	107	143	−56	S22c	2488
Z–1-$C_4H_9 \rightarrow C_4H_{10}$	13	197	−295	94	145	−82	S23c	2334
Z–1-$C_4H_9 \rightarrow C_4H_{10}$	29	207	−285	94	142	−77	–	–
Z–1p-$C_4H_7 \rightarrow$ 1-C_4H_8	88	268	−289	151	174	−38	S24c	1596
Z–1s-$C_4H_7 \rightarrow$ 1-C_4H_8	14	191	−284	112	146	−55	S25c	2031
Z–1s-$C_4H_7 \rightarrow$ 2-C_4H_8	0	177	−284	97	132	−55	S26c	2050
Z–2p-$C_4H_7 \rightarrow$ 2-C_4H_8	7	175	−270	86	99	−21	S27c	2520
Z–$CH_2OH \rightarrow CH_3OH$	−28	157	−298	87	63	38	S28c	2526

[a]Enthalpy and [b]free energies are reported in kJ mol^{-1}, [c]entropy is reported in J K^{-1} mol^{-1}, [d]references the proivded POSCAR/MODECAR files

Table S9. Energies of H_2O-assisted transition states in H-ZSM-5 (MFI), H-SSZ-13 (CHA), and H-SAPO-34 (CHA).

	H-ZSM-5			H-SSZ-13			H-SAPO-34		
State	ΔH	ΔG	ΔS	ΔH	ΔG	ΔS	ΔH	ΔG	ΔS
	kJ mol^{-1}	kJ mol^{-1}	J K^{-1} mol^{-1}						
Z–H + H_2 (g) + H_2O (g)	0	0	0	0	0	0	0	0	0
2-C_4H_8—H_2O	−29	226	−410	−46	221	−429	−23	249	−435
C_4H_6—H_2O	−35	214	−399	−72	187	−417	−44	218	−421
CH_2O—H_2O	−98	170	−430	−112	164	−444	−94	186	−450

Section S8. Images of Transition State Structures

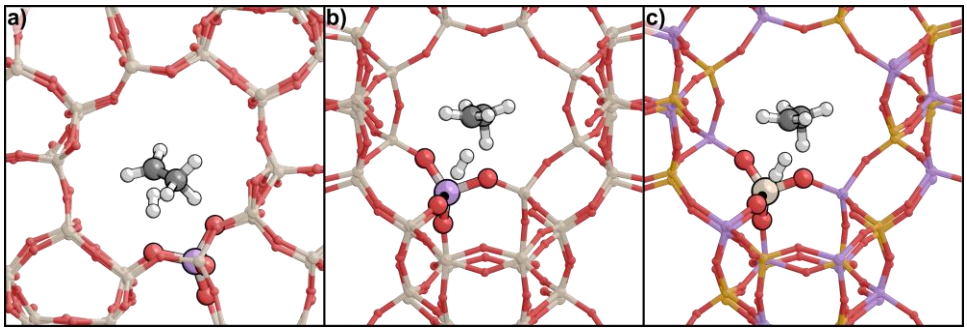

Figure S10. Concerted hydrogenation of ethene in a) H-ZSM-5 (MFI), b) H-SSZ-13 (CHA), and c) H-SAPO-34 (CHA)

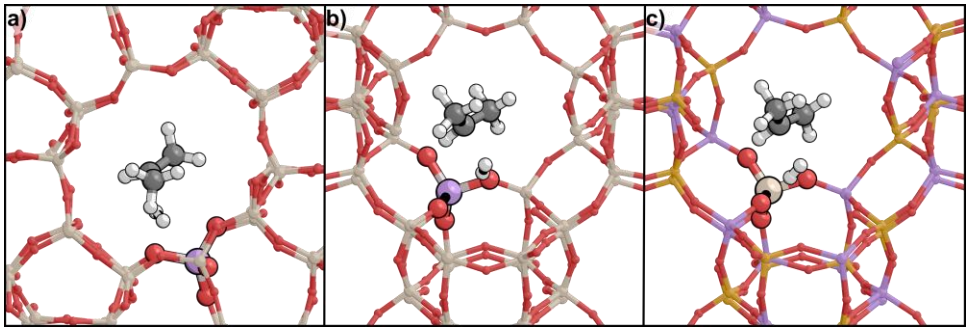

Figure S11. Concerted hydrogenation of propene in a) H-ZSM-5 (MFI), b) H-SSZ-13 (CHA), and c) H-SAPO34 (CHA)

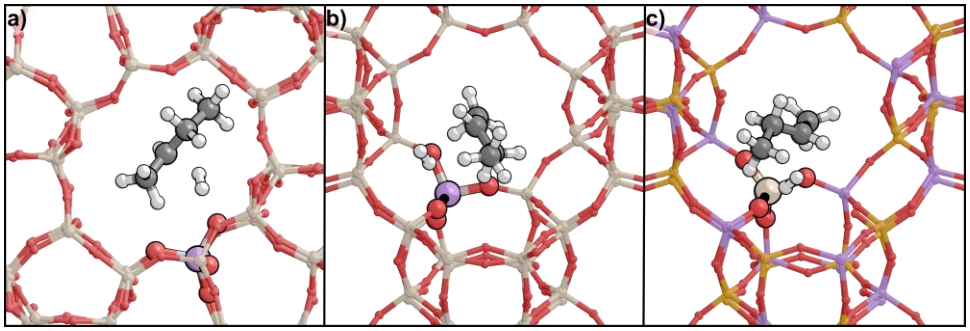

Figure S12. Concerted hydrogenation of 1-butene in a) H-ZSM-5 (MFI), b) H-SSZ-13 (CHA), and c) H-SAPO-34 (CHA)

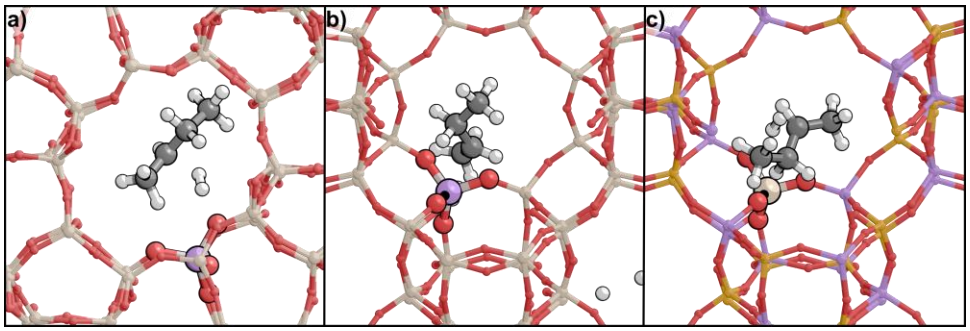

Figure S13. Concerted hydrogenation of 2-butene in a) H-ZSM-5 (MFI), b) H-SSZ-13 (CHA), and c) H-SAPO-34 (CHA)

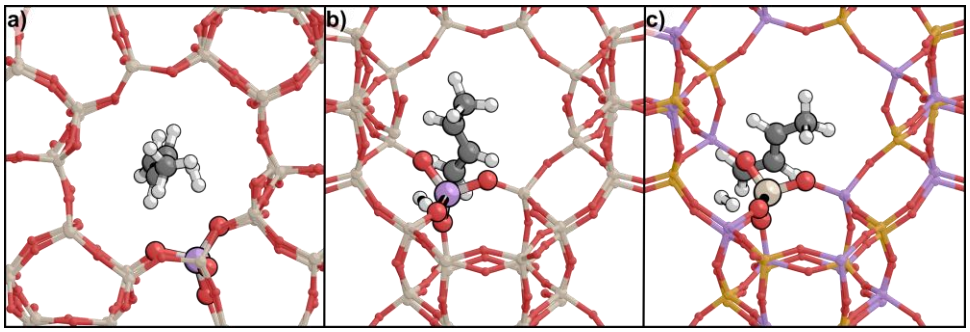

Figure S14. Concerted hydrogenation of butadiene to 1-butene in a) H-ZSM-5 (MFI), b) H-SSZ-13 (CHA), and c) H-SAPO-34 (CHA)

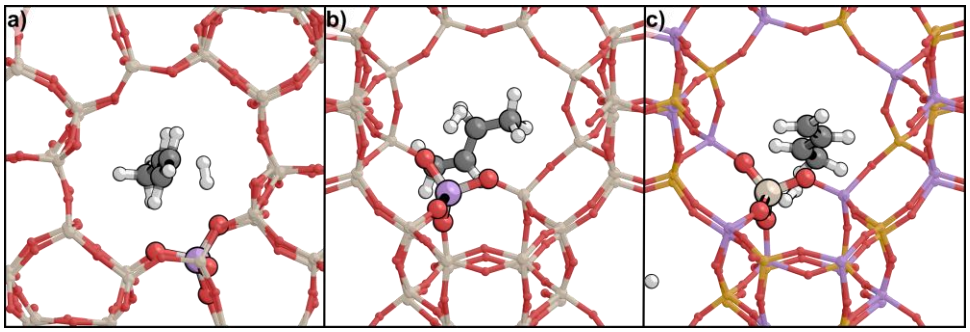

Figure S15. Concerted hydrogenation of butadiene to 2-butene in a) H-ZSM-5 (MFI), b) H-SSZ-13 (CHA), and c) H-SAPO-34 (CHA)

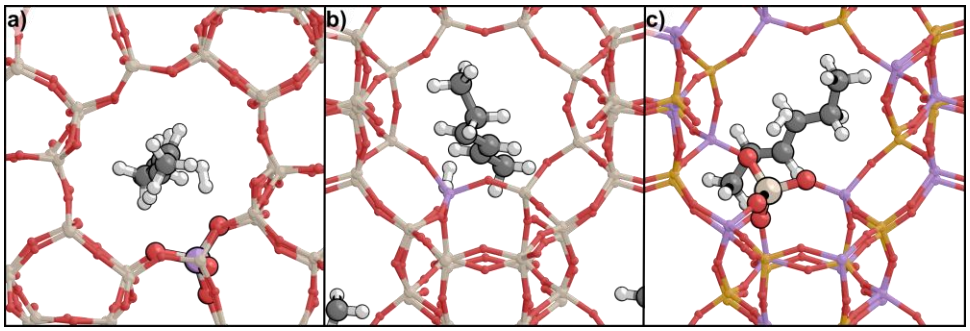

Figure S16. Concerted hydrogenation of hexadiene to 2-hexene in a) H-ZSM-5 (MFI), b) H-SSZ-13 (CHA), and c) H-SAPO-34 (CHA)

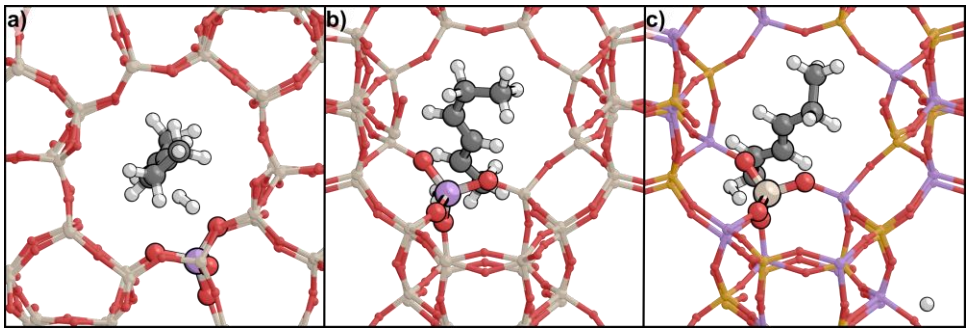

Figure S17. Concerted hydrogenation of hexadiene to 3-hexene in a) H-ZSM-5 (MFI), b) H-SSZ-13 (CHA), and c) H-SAPO-34 (CHA)

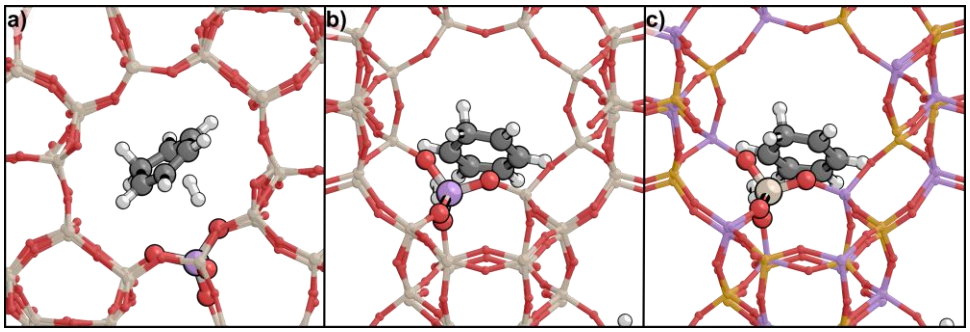

Figure S18. Concerted hydrogenation of benzene in a) H-ZSM-5 (MFI), b) H-SSZ-13 (CHA), and c) H-SAPO-34 (CHA)

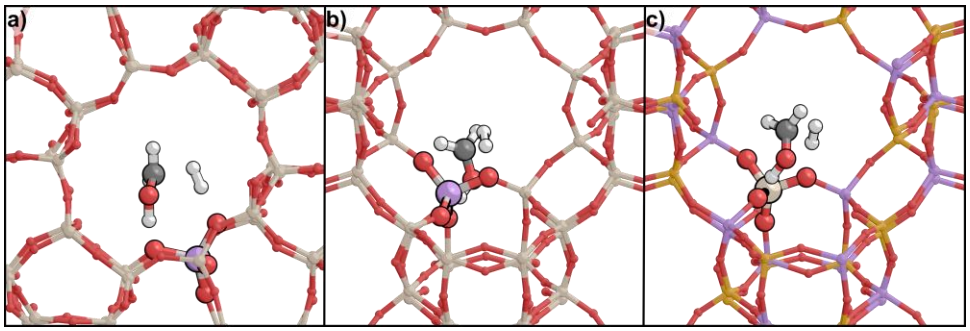

Figure S19. Concerted hydrogenation of CH2O in a) H-ZSM-5 (MFI), b) H-SSZ-13 (CHA), and c) H-SAPO-34 (CHA)

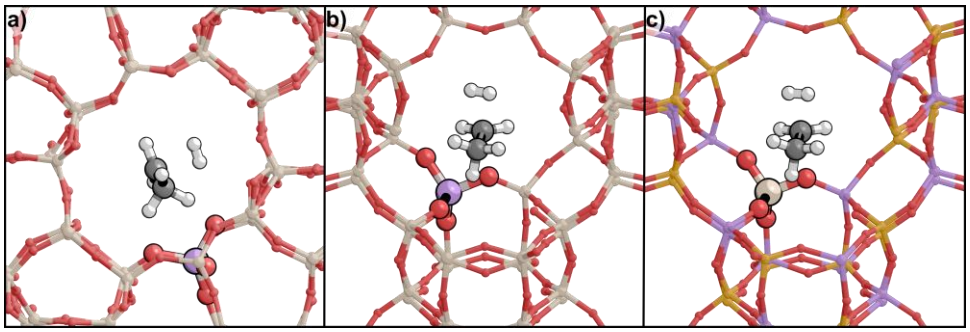

Figure S20. Sequential hydrogenation of Z–C_2H_5 in a) H-ZSM-5 (MFI), b) H-SSZ-13 (CHA), and c) H-SAPO-34 (CHA)

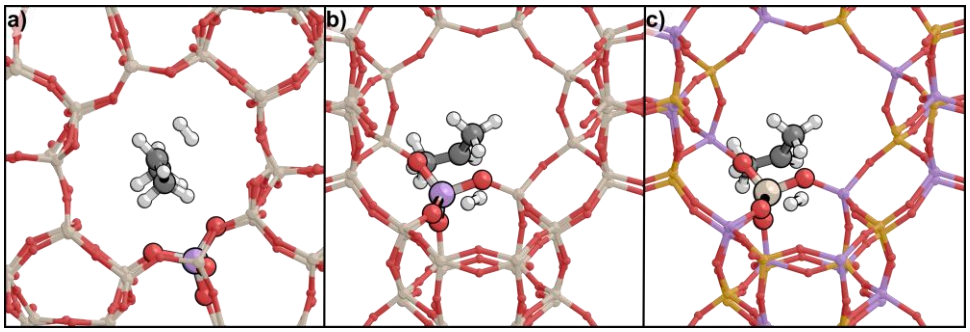

Figure S21. Sequential hydrogenation of Z–C_3H_7 in a) H-ZSM-5 (MFI), b) H-SSZ-13 (CHA), and c) H-SAPO-34 (CHA)

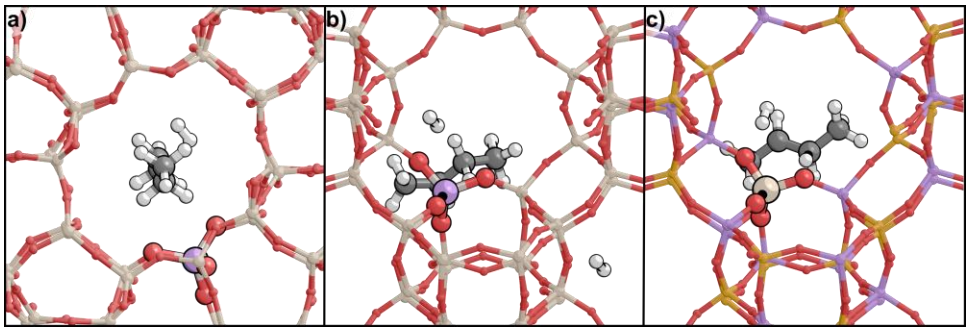

Figure S22. Sequential hydrogenation of Z–2-C_4H_9 in a) H-ZSM-5 (MFI), b) H-SSZ-13 (CHA), and c) H-SAPO-34 (CHA)

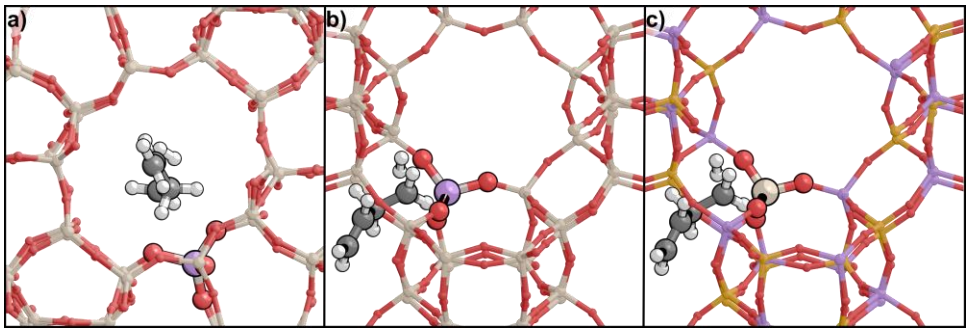

Figure S23. Sequential hydrogenation of Z–1p-C_4H_7 in a) H-ZSM-5 (MFI), b) H-SSZ-13 (CHA), and c) H-SAPO-34 (CHA)

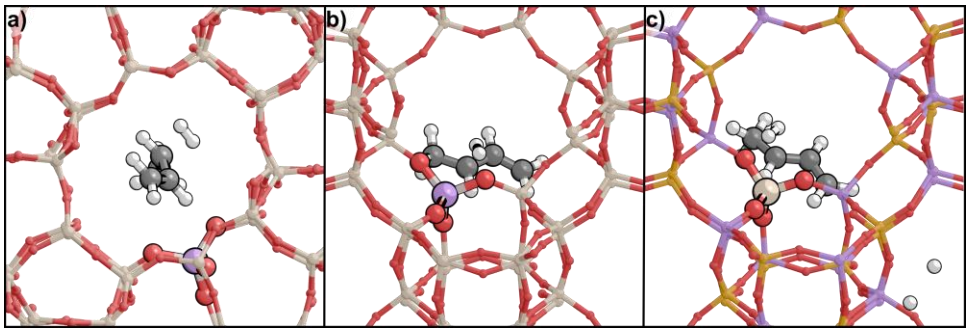

Figure S24. Sequential hydrogenation of Z–1s-C_4H_7 in a) H-ZSM-5 (MFI), b) H-SSZ-13 (CHA), and c) H-SAPO-34 (CHA)

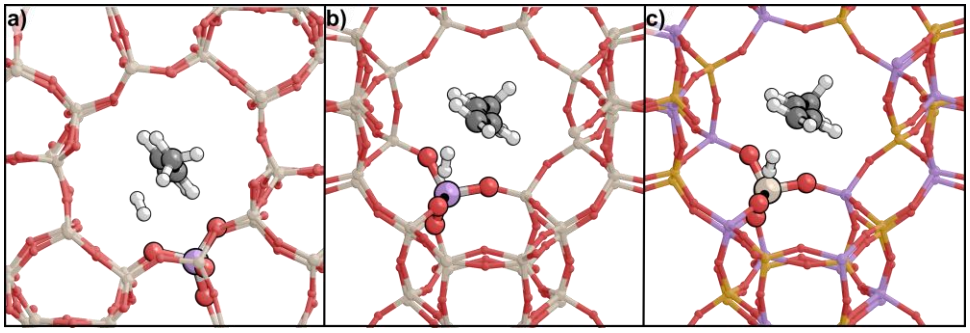

Figure S25. Sequential hydrogenation of Z–2p-C_4H_7 in a) H-ZSM-5 (MFI), b) H-SSZ-13 (CHA), and c) H-SAPO-34 (CHA)

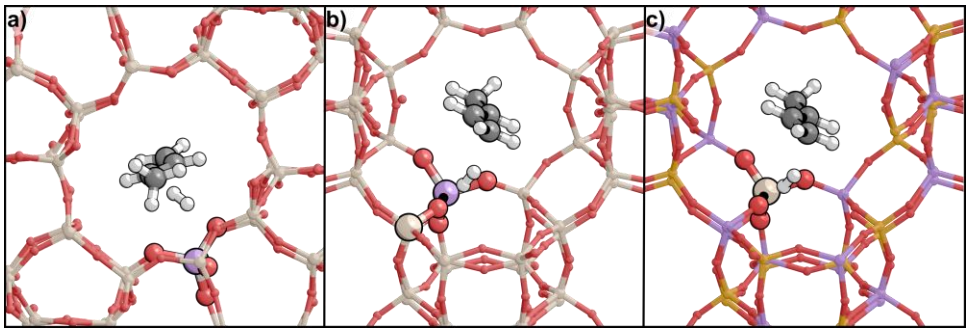

Figure S26. Sequential hydrogenation of Z–2s-C_4H_7 in a) H-ZSM-5 (MFI), b) H-SSZ-13 (CHA), and c) H-SAPO-34 (CHA)

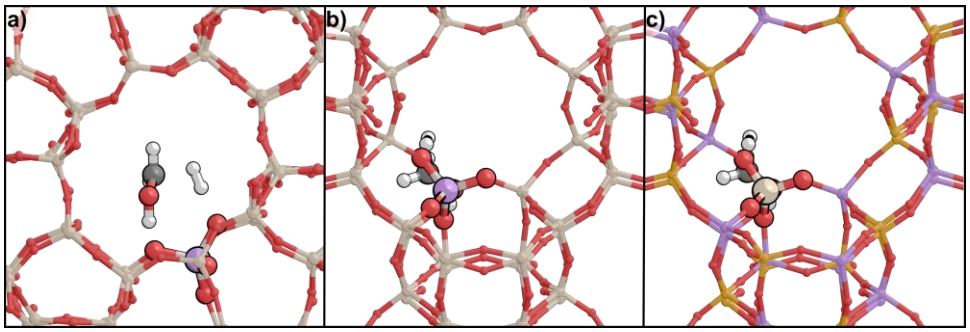

Figure S27. Sequential hydrogenation of Z–CH_2OH in a) H-ZSM-5 (MFI), b) H-SSZ-13 (CHA), and c) H-SAPO-34 (CHA)